Light Curve Modeling and Secular Analyses of the Totally Eclipsing Overcontact Binary System V514 Draconis

Kevin B. Alton
UnderOak Observatory, 70 Summit Avenue, Cedar Knolls, NJ 07927; kbalton@optonline.net

Franz-Josef Hambsch
Oude Bleken 12, Mol, 2400, Belgium; hambsch@telenet.be

Received December 13, 2022; revised March 7, 2023; accepted March 18, 2023

Abstract Precise time-series CCD-derived photometric data (BVR_c) were acquired from V514 Dra at Astrokolhoz Observatory in 2010 and Desert Blooms Observatory in 2022. An updated linear ephemeris was calculated from nine new times of minimum (ToM) produced from this study along with eight other values from the literature. Based on a quadratic fit of residuals from observed and predicted minimum times, secular analyses suggested the orbital period of V514 Dra may be slowly increasing at the rate of $0.0061 \pm 0.0011\ s \cdot y^{-1}$. In addition, simultaneous modeling of new multi-bandpass (BVR_c) light curve data was accomplished using the Wilson-Devinney (WD) code, revealing that V514 Dra is likely a W-subtype overcontact binary (OCB). Since a total eclipse is observed, a photometrically derived value for the mass ratio (q_{ptm}) with acceptable uncertainty could be determined which consequently provided preliminary estimates for selected physical and geometric elements of V514 Dra.

1. Introduction

Sparsely sampled monochromatic photometric data from V514 Dra (=NSVS 1090740) were first captured during the ROTSE-I survey between 1999 and 2000 (Akerlof *et al.* 2000; Wozniak *et al.* 2004). Hoffman *et al.* (2008) initially identified V514 Dra as a new β Lyrae system from the ROTSE-I survey but later (Hoffman *et al.* 2009) re-classified this system as a W UMa-type variable. Lewandowski *et al.* (2009) mis-classified V514 Dra as an Algol-type variable in a study involving 66 other new variable stars discovered by Niedzielski *et al.* (2003). Other sources of photometric data from this eclipsing binary include the sparsely-sampled All-Sky Automated Survey for SuperNovae (ASAS-SN: Shappee *et al.* 2014; Jayasinghe *et al.* 2018) and the Catalina Sky Survey (CSS: Drake *et al.* 2014). Legacy unpublished light curve data (V and I_c) were also obtained from WD30, an AAVSOnet instrument operated at Astrokolhoz Observatory (AO: Cloudcroft, New Mexico, 32.979 N, 105.7334 W) in 2010. Since these light curves were incomplete, they were only used to generate additional times of minimum. Lastly, Korda *et al.* (2017) conducted a photometric investigation (V, R_c, and I_c) of V514 Dra along with 13 other low-mass binaries which included light curve modeling with the Wilson-Devinney (WD) code (Wilson and Devinney 1971; Wilson 1979, 1990). Multi-bandpass (BVR_c) light curves captured from V514 Dra at DBO in 2022 were synthesized using the same Roche-lobe modeling code.

2. Observations and data reduction

Precise time-series photometric observations were obtained in 2022 at Desert Blooms Observatory (DBO, USA, 31.941 N, 110.257 W) using a QSI 683 wsg-8 CCD camera mounted at the Cassegrain focus of an 0.4-m Schmidt-Cassegrain telescope. This focal-reduced (f/7.2) instrument produces an image scale of 0.76 arcsec/pixel (bin=2×2) and a field of view (FOV) of 15.9×21.1 arcmin. The CCD camera was equipped with photometric B, V, and R_c filters manufactured to match the Johnson-Cousins Bessell specification. Image (science, darks, and flats) acquisition software (TheSkyX Pro Edition 10.5.0; Software Bisque 2019) controlled the main and off-axis guide cameras. Image acquisition at AO was accomplished using MaxIm DL 5.07 (Diffraction Limited. 2012) to control an SBIG ST-9 CCD detector (V and I_c passbands) that was mounted at the Cassesgrain focus of an LX-200 (12") optical tube assembly. Dark subtraction, flat correction, and registration of all images were performed prior to any analysis. Instrumental readings were reduced to catalog-based magnitudes using APASS DR9 values (Henden *et al.* 2009, 2010, 2011; Smith *et al.* 2011) built into MPO Canopus v 10.7.12.9 (Minor Planet Observer 2010). Light curve data acquired at AO were similarly reduced to APASS DR9 values using LesvePhotometry V1.2.0.137 (de Ponthière 2010).

Magnitude values for photometric data were produced from two comparison stars (DBO: GSC 4421-0175 and GSC 4421-0197; AO: GSC 4421-0175 and GSC 4421-0399) which on average remained constant throughout every imaging session. The identity, J2000 coordinates, and color indices (B–V) for these stars are provided in Table 1. An AAVSO finder chart annotated with the location of the target (T) and comparison stars (1–3) is reproduced in Figure 1. Only data acquired above 30° altitude (airmass < 2.0) were evaluated; considering the close proximity of all program stars, differential atmospheric extinction was ignored. All photometric data acquired by co-author Hambsch from V514 Dra at AO (2010) and co-author Alton at DBO (2022) can be retrieved from the AAVSO International Database (Kafka 2021).

3. Results and discussion

Results and a detailed discussion about the determination of linear and quadratic ephemerides are provided in this section.

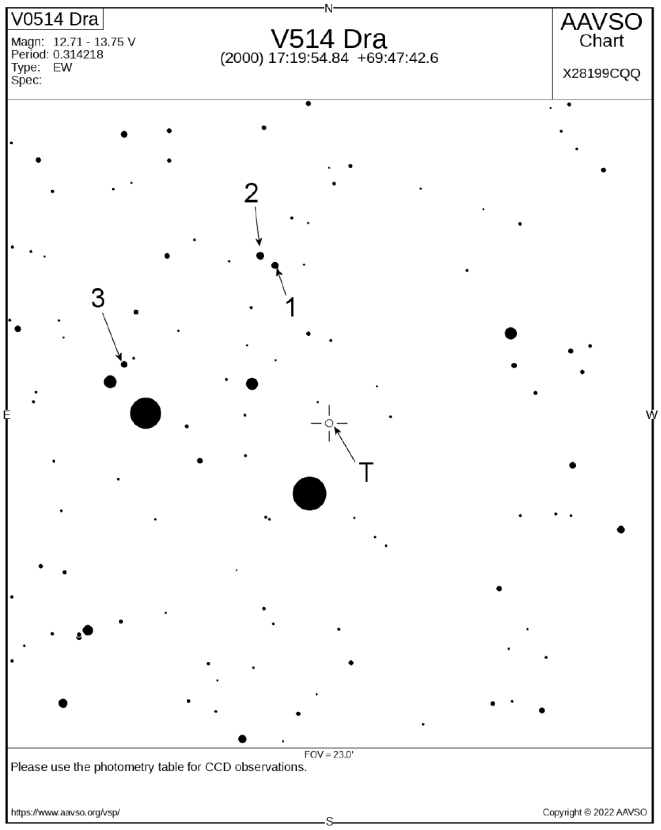

Figure 1. Finder chart for V514 Dra (T) also showing the comparison stars (1–3) used for aperture-derived photometery and generation of APASS DR9-derived magnitude estimates.

Table 1. Astrometric coordinates, V-magnitudes, and color indices (B–V) for V514 Dra, and the corresponding comparison stars (Figure 1) used in this photometric study.

Star Identification	*R.A. (J2000)*[a] *h m s*	*Dec. (J2000)*[a] *° ′ ″*	*V-mag*[b]	*(B–V)*[b]
(1) GSC 4421-0175[c,d]	17 20 23.2704	+69 53 39.228	12.074	0.472
(2) GSC 4421-0197[c]	17 20 17.1648	+69 53 18.852	12.455	0.385
(3) GSC 4421-0399[d]	17 21 19.3656	+69 49 46.740	12.711	0.535
(T) V514 Dra	17 19 54.8279	+69 47 42.649	12.976	0.662

[a] *R.A. and Dec. from Gaia EDR3 (Gaia Collab.* et al. *2021)*
[b] *V-mag and (B–V) for comparison stars derived from APASS DR9 database described by Henden* et al. *(2009, 2010, 2011) and Smith* et al. *(2011).*
[c] *Comparison stars used for DBO data.*
[d] *Comparison stars used for AO data.*

Thereafter, a multi-source approach for estimating the effective temperature of V514 Dra along with Roche-lobe modeling with the WD code are examined. Finally, preliminary estimates for mass ($M_\odot$) and radius ($R_\odot$) along with corresponding calculations for luminosity ($L_\odot$), surface gravity (log (g)), semi-major axis (a), and bolometric magnitude (M_{bol}) are derived.

3.1. Photometry and ephemerides

A total of 274 photometric values in B, 309 in V, and 300 in R_c passbands were acquired from V514 Dra at DBO between 2022 March 3 and 2022 March 27. Photometric uncertainty, which typically remained within ± 0.005, was calculated according to the so-called "CCD Equation" (Mortara and Fowler 1981; Howell 2006). The 2010 imaging campaign (2010 April 4–2010 April 25) at AO provided an additional 446 values in V and 149 readings in I_c bandpass which were only used to supplement ToM values needed for secular analysis of the orbital period. ToM values and associated errors from data acquired at DBO and AO were calculated according to Andrych and Andronov (2019) and Andrych *et al.* (2020) using the program MAVKA (Andrych *et al.* 2020). Simulations of extrema were automatically optimized by finding the most precise degree (α) and best fit algebraic polynomial expressions. ToM differences (ETD) vs. epoch were fit using scaled Levenberg-Marquardt algorithms (QtiPlot 0.9.9-rc9; IONDEV SRL 2021).

Table 2. V514 Dra times-of-minimum (HJD: 2006 March 23–2022 March 27), cycle number, and eclipse timing difference (ETD) between observed and predicted times derived from the updated linear ephemeris (Equation 1).

HJD = 2400000+	*HJD Error*	*Cycle No.*	*ETD*	*Ref.*
53817.7773	0.0000	–18611	0.0004	1
54210.8662	0.0010	–17360	0.0019	2
55291.9336	0.0002	–13919.5	0.0007	3
55293.9766	0.0002	–13913	0.0012	3
55311.8869	0.0002	–13856	0.0011	3
55721.7832	0.0005	–12551.5	–0.0006	4
57089.4184	0.0003	–8199	–0.0014	5
57126.4962	0.0008	–8081	–0.0013	5
57126.6532	0.0009	–8080.5	–0.0015	5
57142.3643	0.0002	–8030.5	–0.0013	5
57147.3919	0.0005	–8014.5	–0.0012	5
57177.3994	0.0004	–7919	–0.0016	5
57890.0472	0.0010	–5651	–0.0013	6
59644.0178	0.0002	–69	0.0017	7
59663.8129	0.0002	–6	0.0011	7
59663.9703	0.0002	–5.5	0.0013	7
59665.8551	0.0002	0.5	0.0008	7

References: (1) Lewandowski et al. *(2009); (2) CSS (Drake* et al. *2014); (3) AO: this study; (4) Diethelm (2011); (5) Korda* et al. *(2017); (6) ASAS-SN (Shappee* et al. *2014; Jayasinghe* et al. *2018); (7) DBO: this study.*

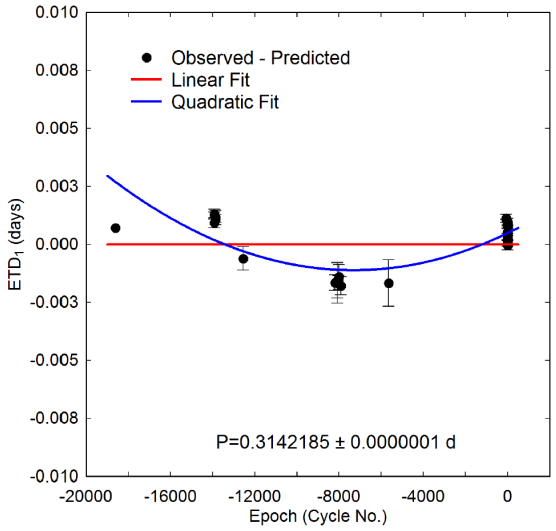

Figure 2. Linear and quadratic fit of ToM differences (ETD_1) vs. epoch for V514 Dra calculated using the new linear ephemeris (Equation 1). Measurement uncertainty is denoted by the error bars.

Seven new ToM values were derived from photometric data acquired at DBO and AO. An additional ToM value was extrapolated from the ASAS-SN and Catalina Sky surveys along with eight other observations gathered from the literature (Table 2). A new linear ephemeris (HJD) based on near-term (2017–2022) results was determined as follows:

$$\text{Min. I(HJD)} = 2459665.6978(4) + 0.314219(1)\,E \quad (1)$$

The difference (ETD) between observed eclipse times (Figure 2) and those predicted by the linear ephemeris against epoch (cycle number) reveals what appears to be a quadratic relationship where:

$$\text{ETD} = 1.0668 \pm 0.3903 \cdot 10^{-3} + 5.0325 \pm 0.98205 \cdot 10^{-7}E + 3.0179 \pm 0.5552 \cdot 10^{-11}E^2 . \quad (2)$$

Given that the quadratic term coefficient (Q=3.0179±0.5552) is positive, this result would suggest that the orbital period has been increasing at the rate ($dP/dt = 2Q/P$) of $0.0061 \pm 0.0011\ s \cdot y^{-1}$. This rate, albeit slow, falls within those reported from many other overcontact systems in the literature (Latković *et al.* 2021). Period change over time that can be described by a parabolic expression is often attributed to mass transfer or by angular momentum loss (AML) due to magnetic stellar wind (Qian 2001, 2003; Li *et al.* 2019). Ideally the net effect is a decreasing orbital period when AML dominates. When conservative mass transfer from the more massive to its less massive binary partner prevails, then the orbital period can also decrease. Separation increases when conservative mass transfer from the less massive to its more massive cohort occurs or when spherically symmetric mass loss from either body (e.g. a wind but not magnetized) takes place. In mixed situations (e.g. mass transfer from less massive star, together with AML) the orbit evolution depends on which process dominates.

3.2. Effective temperature estimation

The primary star is herein defined as the more massive, and therefore more luminous component. In the absence of a published medium to high resolution UV-vis spectrum, T_{eff1} was derived from a composite (USNO-A2, 2MASS, APASS, UCAC4) of photometric determinations that were as appropriate transformed to (B–V)[1,2]. Interstellar extinction ($A_V = 0.1026 \pm 0.0016$) and reddening ($E(B–V) = A_V/3.1$) were estimated according to a galactic dust map model derived by Schlafly and Finkbeiner (2011). Additional sources used to establish a mean value for T_{eff1} included the Gaia DR2 release of stellar parameters (Andrae *et al.* 2018) and an empirical relationship (Houdashelt *et al.* 2000) based on intrinsic color, $(B–V)_0$. The mean result ($T_{eff1} = 5390 \pm 239$ K) was adopted for WD modeling of light curves from V514 Dra (Table 3).

3.3. Light curve modeling with the Wilson-Devinney Code

Roche-lobe modeling of light curve data (Figure 3) acquired in 2022 (DBO) was initially performed with PHOEBE 0.31a (Prša and Zwitter 2005) and then refined using WDwint56a (Nelson 2009). Both programs feature a graphical interface to the Wilson-Devinney WD2003 code (Wilson and Devinney 1971; Wilson 1979, 1990). WDwint56a incorporates Kurucz's atmosphere models (Kurucz 2002) that are integrated over BVR_c passbands. Most commonly, W-subtype OCBs (Binnendijk 1970) have been shown to have a relatively cool effective temperature (late G to early K spectral class) and an orbital period less than 0.4 d. Based on this assumption, Roche-lobe modeling of the DBO (Figure 3) light curves initially proceeded using Mode 3 for an overcontact binary; other modes (detached and semi-detached) never improved light curve simulation as defined by the model residual mean square errors. Since the effective temperature of the primary was estimated to be 5390 K, internal energy transfer to the stellar surface is driven

Table 3. Estimation of the primary star effective temperature (T_{eff1}) for V514 Dra.

Parameter	*Value*
DBO $(B–V)_0$[a]	0.608 ± 0.033
Mean combined $(B–V)_0$[a]	0.727 ± 0.135
Galactic reddening E(B–V)[b]	0.0331 ± 0.0005
Survey T_{eff1}[c] (K)	5506 ± 391
Gaia T_{eff1}[d] (K)	5165^{-144}_{+366}
Houdashelt T_{eff1}[e] (K)	5495 ± 477
Mean T_{eff1} (K)	5390 ± 239
Spectral Class[f].	G8V-G9V

[a] *DBO and mean combined intrinsic $(B–V)_0$ determined using reddening value (E(B–V)).*
[b] *https://irsa.ipac.caltech.edu/applications/DUST/*
[c] *T_{eff1} interpolated from mean combined $(B–V)_0$ using Table 4 in Pecaut and Mamajek (2013).*
[d] *Values from Gaia DR2 (Gaia Collab. 2016, 2018; http://vizier.u-strasbg.fr/viz-bin/VizieR?- source=I/345/gaia2).*
[e] *Values calculated with Houdashelt* et al. *(2000) empirical relationship.*
[f] *Spectral class estimated from Pecaut and Mamajek (2013) based on mean T_{eff}*

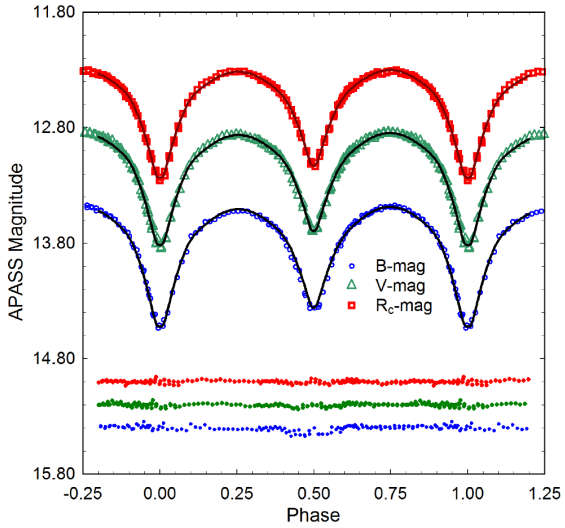

Figure 3. Period-folded (0.3142189 ± 0.0000001 d) CCD-derived light curves for V514 Dra produced from photometric data collected at DBO between 2022 March 3 and 2022 March 27. The top (R_c), middle (V), and bottom curves (B) were transformed to magnitudes based on APASS DR9-derived catalog values from comparison stars. In this case, the model assumed a W-subtype overcontact binary with a cool spot on the primary star; residuals from the model fits are offset at the bottom of the plot to compress the y-axis.

[1] http://www.aerith.net/astro/color_conversion.html
[2] http://brucegary.net/dummies/method0.html

by convective (<7200 K) rather than by radiative processes (Bradstreet and Steelman 2004). Therefore, bolometric albedo ($A_{1,2}$ = 0.5) was assigned according to Ruciński (1969), while the gravity darkening coefficient ($g_{1,2}$ = 0.32) was adopted from Lucy (1967). Logarithmic limb darkening coefficients (x_1, x_2, y_1, y_2) were interpolated (Van Hamme 1993) following any change in effective temperature during model fit optimization by differential corrections (DC). All but the temperature of the more massive star (T_{eff1}), $A_{1,2}$, and $g_{1,2}$ were allowed to vary during DC iterations. In general, the best fits for T_{eff2}, i, q, and Roche potentials ($\Omega_1 = \Omega_2$) were collectively refined (method of multiple subsets) by DC using the multi-bandpass light curve data until a simultaneous solution was found. Light curve data acquired at DBO in 2022 (Figure 3) showed an obvious asymmetry during quadrature (Max I < Max II). This so-called "O'Connell effect" (O'Connell 1951) assumes some sort of surface inhomogeneity often associated with star spots. In this case the addition of a single cool spot positioned on the primary star provided the best fit light curve models. Furthermore, V514 Dra did not require any third light correction (l_3 = 0) to improve WD model fits.

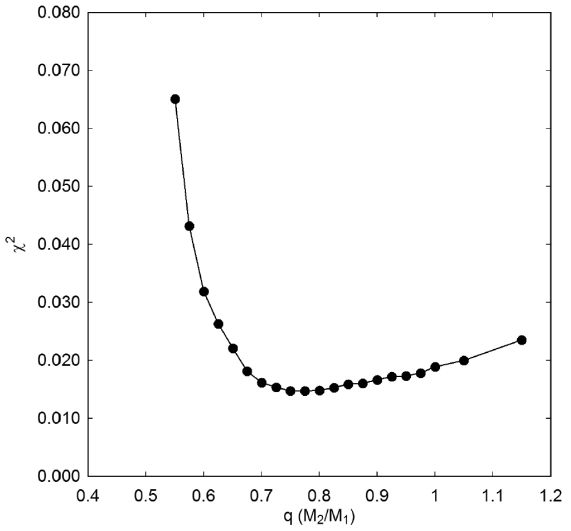

Figure 4. A "q-search" assessment using PHOEBE v0.31a during which the best Roche-lobe model fit was determined using differential corrections after fixing a value for the mass ratio (q) between 0.55 and 1.15 and then varying i, $\Omega_{1,2}$, and T_{eff2}.

3.4. Wilson-Devinney modeling results

It is generally not possible to unambiguously determine the mass ratio or total mass of an eclipsing binary system without spectroscopic radial velocity (RV) data. In this case, an obvious flattened bottom during minimum light that is usually indicative of a total eclipse was not observed. Nonetheless, a total eclipse is still possible when two similarly sized binary stars are viewed edge on (i ≈ 90°). With totality, degeneracy between the radii and inclination is broken (Terrell and Wilson 2005; Terrell 2022) such that a mass ratio can be determined with very small (< 1%) relative error (Liu 2021). To address this potential concern, an exhaustive "q-search" analysis was conducted in which values of the mass ratio ranging between 0.55 and 1.15 were fixed during WD modeling in order to find the best fit (χ^2) using differential corrections while changing i, $\Omega_{1,2}$, and T_{eff2}. As can be seen in Figure 4, mean model residuals using the MAO light curve data (B, V, and R_c) reach a minimum when q ≈ 0.75.

Standard errors reported in Table 4 are computed from the DC covariance matrix and only reflect the model fit to the observations which assume exact values for any fixed parameter. These formal errors are generally regarded as unrealistically small, considering the estimated uncertainties associated with the mean adopted T_{eff1} values along with basic assumptions about $A_{1,2}$, $g_{1,2}$, the influence of spots added to the WD model, and immeasurable total experimental error. Normally, the value for T_{eff1} is fixed with no error during modeling with the WD code. When T_{eff1} is varied by as much as ± 10%, investigations with other OCBs including A- (Alton 2019; Alton *et al.* 2020) and W-subtypes (Alton and Nelson 2018) have shown that uncertainty estimates for i, q, or $\Omega_{1,2}$ were not appreciably (<2.5%) affected. Assuming that the actual T_{eff1} value falls within ± 10% of the adopted values used for WD modeling (not unreasonable based on T_{eff1} data provided in Table 3), then uncertainty estimates for i, q, or $\Omega_{1,2}$ along with spot size, temperature, and location would likely not exceed this amount.

Table 4. Light curve parameters evaluated by WD modeling and the geometric elements derived for V514 Dra assuming it is a W-type W UMa variable.

Parameter[a]	*DBO No Spot*	*DBO Spotted*
T_{eff1} (K)[b]	5390 (239)	5390 (239)
T_{eff2} (K)	5598 (248)	5597 (248)
q (m_2/m_1)	0.76 (1)	0.75 (1)
A[b]	0.50	0.50
g[b]	0.32	0.32
$\Omega_1 - \Omega_2$	3.28 (1)	3.26 (1)
i°	88.9 (19)	89.6 (7)
$A_P = T_S/T_\star$[c]	—	0.89 (1)
Θ_P (spot co-latitude)[c]	—	101 (5)
φ_P (spot longitude)[c]	—	119 (3)
r_P (angular radius)[c]	—	15 (3)
$L_1/(L_1+L_2)_B$[d]	0.503 (1)	0.504 (1)
$L_1/(L_1+L_2)_V$	0.518 (1)	0.519 (1)
$L_1/(L_1+L_2)_{Rc}$	0.526 (1)	0.526 (1)
r_1 (pole)	0.389 (1)	0.390 (1)
r_1 (side)	0.412 (1)	0.414 (1)
r_1 (back)	0.446 (1)	0.449 (1)
r_2 (pole)	0.343 (2)	0.343 (2)
r_2 (side)	0.360 (2)	0.361 (2)
r_2 (back)	0.398 (3)	0.399 (4)
Fill-out factor (%)	15.2	17.0
RMS (B)[e]	0.01601	0.01362
RMS (V)	0.01048	0.00871
RMS (R_c)	0.00853	0.00838

[a] *All uncertainty estimates for q, $\Omega_{1,2}$, i, $r_{1,2}$, and L_1 from WDwint56A (Nelson 2009).*
[b] *Fixed with no error during DC.*
[c] *Primary star spot parameters in degrees (Θ_P, φ_P, and r_P); A_P equals the spot temperature (T_S) divided by star temperature, $T_\star$.*
[d] *L_1 and L_2 refer to scaled luminosities of the primary and secondary stars, respectively.*
[e] *Monochromatic residual mean square error from observed values.*

The fill-out parameter (f) which corresponds to the outer surface shared by each star was calculated according to Kallrath and Malone (2009) and Bradstreet (2005) where:

$$f = (\Omega_{inner} - \Omega_{1,2}) / (\Omega_{inner} - \Omega_{outer}), \quad (3)$$

wherein Ω_{outer} is the outer critical Roche equipotential, Ω_{inner} is the value for the inner critical Roche equipotential, and $\Omega = \Omega_{1,2}$ denotes the common envelope surface potential for the binary system. In this case V514 Dra is considered overcontact since $0 < f < 1$.

Spatial renderings (Figure 5) were produced with Binary Maker 3 (BM3: Bradstreet and Steelman 2004) using the final WDwint56a modeling (BVR_c) results from 2022. The smaller secondary is shown to fully transit across the primary face during Min II ($\varphi = 0.5$), thereby confirming that the secondary star is totally eclipsed at Min I.

An earlier (2015–2016) multi-bandpass (VR_cI_c) CCD study on V514 Dra (Korda *et al.* 2017) produced modeling results that were quite disparate from those generated herein. Aside from a large difference in the adopted T_{eff} (4750 vs. 5390 K) for the primary star, estimates for the mass ratio (1 vs. 0.75) and related parameters ($R_\odot$, $L_\odot$, M_{bol}, and Log (g)) suggested that both stars are nearly identical in size and temperature. This is in contrast to the corresponding estimates summarized in Table 5 which indicate that both stars are distinctly different. Obviously a radial velocity (RV) study could reconcile which light curve solution is closest to the true fit.

3.5. Preliminary stellar parameters

Mean physical characteristics were estimated for V514 Dra (Table 5) using results from the best fit (spotted) light curve simulations from 2022. Without the benefit of RV data which define the orbital motion, mass ratio, and total mass of the binary pair, these results should be considered "relative" rather than "absolute" parameters and regarded as preliminary. Nonetheless, since the photometric mass ratio (q_{ptm}) is derived from a totally eclipsing OCB, there is a reasonable expectation that DC optimization with the WD2003 code would have arrived at a solution with acceptable uncertainty for q (Terrell and Wilson 2005; Liu 2021; Terrell 2022).

Calculations are described below for estimating the solar mass and size, semi-major axis, solar luminosity, bolometric V-mag, and surface gravity of each component. Four empirically derived mass-period relationships (M-PR) for W UMa-type binaries were used to estimate the primary star mass. The first M-PR was reported by Qian (2003), others followed from Gazeas and Stępień (2008), Gazeas (2009), and more recently Latković *et al.* (2021). According to Qian (2003), when the primary star is less than 1.35 $M_\odot$ or the system is W-type its mass can be determined from:

$$M_1 = 0.391(59) + 1.96(17) \cdot P, \quad (4)$$

where P is the orbital period in days. This leads to $M_1 = 1.007 \pm 0.080\ M_\odot$ for the primary.

The M-PR derived by Gazeas and Stępień (2008):

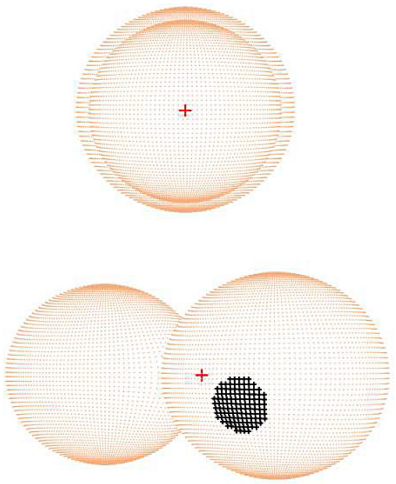

Figure 5. A spatial model of V514 Dra observed at DBO during 2022 illustrating (bottom) location of the cool (black) spot on the primary star and (top) the secondary star transit across the primary star face at Min II ($\varphi = 0.5$).

Table 5. Fundamental stellar parameters for V514 Dra using the photometric mass ratio ($q_{ptm} = m_2/m_1$) from the spotted WD model fits of light curve data (DBO) and the estimated primary star mass based on four empirically derived M-PRs for overcontact binary systems.

Parameter	*Primary*	*Secondary*
Mass ($M_\odot$)	1.05 ± 0.04	0.79 ± 0.03
Radius ($R_\odot$)	0.96 ± 0.01	0.85 ± 0.01
a ($R_\odot$)	2.38 ± 0.02	2.38 ± 0.02
Luminosity ($L_\odot$)	0.70 ± 0.13	0.63 ± 0.11
M_{bol}	5.13 ± 0.02	5.25 ± 0.19
Log (g)	4.49 ± 0.02	4.48 ± 0.02

$$\log(M_1) = 0.755(59) \cdot \log(P) + 0.416(24), \quad (5)$$

corresponds to an OCB system where $M_1 = 1.087 \pm 0.096\ M_\odot$.

Gazeas (2009) reported another empirical relationship for the more massive (M_1) star of a contact binary such that:

$$\log(M_1) = 0.725(59) \cdot \log(P) - 0.076(32) \cdot \log(q) + 0.365(32). \quad (6)$$

from which $M_1 = 1.023 \pm 0.062\ M_\odot$.

Finally, Latković *et al.* (2021) conducted an exhaustive analysis from nearly 700 W UMa stars in which they established mass-period, radius-period, and luminosity-period relationships for the primary and secondary stars. Accordingly, the M-PR:

$$M_1 = (2.94 \pm 0.21 \cdot P) + (0.16 \pm 0.08). \quad (7)$$

leads to a primary star mass of $1.084 \pm 0.104\ M_\odot$.

The mean result from these four values ($M_1 = 1.05 \pm 0.04\ M_\odot$) was used for subsequent determinations of M_2, semi-major axis a, volume-radii r_L, and bolometric magnitudes (M_{bol}) using the formal errors calculated by WDWint56a (Nelson 2009). The secondary mass ($0.79 \pm 0.03\ M_\odot$) and total mass ($1.84 \pm 0.05\ M_\odot$) were determined using the photometric mass ratio ($q_{ptm} = 0.75 \pm 0.01$) derived from the best fit (spotted) model obtained from the DBO light curves.

The semi-major axis, $a(R_\odot) = 2.38 \pm 0.02$, was calculated from Newton's version of Kepler's third law where:

$$a^3 = (G \cdot P^2 (M_1 + M_2)) / (4\pi^2). \quad (8)$$

The effective radius of each Roche lobe (r_L) can be calculated over the entire range of mass ratios ($0 < q < \infty$) according to an expression derived by Eggleton (1983):

$$r_L = (0.49q^{2/3}) / (0.6q^{2/3} + \ln(1 + q^{1/3})), \quad (9)$$

from which values for r_1 (0.4037 ± 0.0004) and r_2 (0.3546 ± 0.0004) were determined for the primary and secondary stars, respectively. The radii in solar units for both binary components can be calculated such that $R_1 = a \cdot r_1 = 0.96 \pm 0.01\, R_\odot$ and $R_2 = a \cdot r_2 = 0.85 \pm 0.01\, R_\odot$.

Luminosity in solar units ($L_\odot$) for the primary (L_1) and secondary stars (L_2) was calculated from the well-known relationship derived from the Stefan-Boltzmann law where:

$$L_{1,2} = (R_{1,2} / R_\odot)^2 (T_{1,2} / T_\odot)^4. \quad (10)$$

Assuming that $T_{eff1} = 5390$ K, $T_{eff2} = 5597$ K, and $T_\odot = 5772$ K, then the solar luminosities ($L_\odot$) for the primary and secondary are $L_1 = 0.70 \pm 0.13$ and $L_2 = 0.63 \pm 0.11$, respectively.

4. Conclusions

This investigation of V514 Dra has expanded the list of totally eclipsing W UMa-type variables that have been provisionally characterized using a photometrically derived mass ratio. Like many other W-subtype OCBs, V514 Dra is comprised of two relatively cool (late spectral class G) stars with an orbiting period less than 0.4 d. Seven new ToM values were determined from light curves acquired at AO in 2010 and DBO in 2022. These values were supplemented with a single value extrapolated from both the ASAS-SN (2017) and CSS (2007) surveys along with eight others reported in the literature. Based on a quadratic fit of residuals from observed and predicted minimum times, secular analyses suggested the orbital period of V514 Dra may be slowly increasing at the rate of 0.0061 ± 0.0011 $s \cdot y^{-1}$. The photometric mass ratio ($q_{ptm} = 0.75 \pm 0.01$) determined by WD modeling is expected to compare favorably with a mass ratio (q_{sp}) derived from RV data. Nevertheless, spectroscopic studies (RV and high resolution classification spectra) will be required to unequivocally determine a total mass and spectral class for this binary system. Consequently, all parameter values and corresponding uncertainties reported herein should be considered preliminary.

5. Acknowledgements

This research has made use of the SIMBAD database operated at Centre de Données astronomiques de Strasbourg, France. In addition, the All-Sky Automated Survey for Supernovae (https://asas-sn.osu.edu/variables), Catalina Sky Survey (http://nesssi.cacr.caltech.edu/DataRelease/), and the AAVSO International Variable Star Index (Watson *et al.* 2014) were mined for essential information. This work also presents results from the European Space Agency (ESA) space mission Gaia. Gaia data are being processed by the Gaia Data Processing and Analysis Consortium (DPAC). Funding for the DPAC is provided by national institutions, in particular the institutions participating in the Gaia MultiLateral Agreement (MLA). The Gaia mission website is https://www.cosmos.esa.int/gaia. The Gaia archive website is https://archives.esac.esa.int/gaia. This research was made possible through use of the AAVSO Photometric All-Sky Survey (APASS), funded by the Robert Martin Ayers Sciences Fund.

Many thanks to the anonymous referee and Editor Morrison, both of whom provided valuable commentary along with corrections.

References

Akerlof, C., *et al.* 2000, *Astron. J.*, **119**, 1901.
Alton, K. B. 2019, *J. Amer. Assoc. Var. Star Obs.*, **47**, 7.
Alton, K. B., and Nelson, R. H. 2018, *Mon. Not. Roy. Astron. Soc.*, **479**, 3197.
Alton, K. B., Nelson, R. H., and Stępień, K. 2020, *J. Astrophys. Astron.*, **41**, 26.
Andrae, R., *et al.* 2018, *Astron. Astrophys.*, **616A**, 8.
Andrych, K. D., and Andronov, I. L. 2019, *Open Eur. J. Var. Stars*, **197**, 65.
Andrych, K. D., Andronov, I. L., and Chinarova, L. L. 2020, *J. Phys. Stud.*, **24**, 1902 (https://uavso.org.ua/mavka/).
Binnendijk, L. 1970, *Vistas Astron.*, **12**, 217.
Bradstreet, D. H., and Steelman, D. P. 2004, Binary Maker 3, Contact Software (http://www.binarymaker.com).
Bradstreet, D. H. 2005, in *The Society for Astronomical Sciences 24th Annual Symposium on Telescope Science*, Society for Astronomical Sciences, Rancho Cucamonga, CA, 23.
de Ponthière, P. 2010, LesvePhotometry, automatic photometry software (http://www.dppobservatory.net).
Diethelm, R. 2011, *Inf. Bull. Var. Stars*, No. 5992, 1.
Diffraction Limited. 2023, MaxIm DL image processing software (http://www.cyanogen.com).
Drake, A. J., *et al.* 2014, *Astrophys. J., Suppl. Ser.*, **213**, 9.
Eggleton, P. P. 1983, *Astrophys. J.,* **268**, 368.
Gaia Collaboration, *et al.* 2016, *Astron. Astrophys.*, **595A**, 1.
Gaia Collaboration, *et al.* 2018, *Astron. Astrophys.*, **616A**, 1.
Gaia Collaboration, *et al.* 2021, *Astron. Astrophys.*, **649A**, 1.
Gazeas, K. D. 2009, *Commun. Asteroseismology*, **159**, 129.
Gazeas, K., and Stępień, K. 2008, *Mon. Not. Roy. Astron. Soc.*, **390**, 1577.
Henden, A. A., Levine, S. E., Terrell, D., Smith, T. C., and Welch, D. L. 2011, *Bull. Amer. Astron. Soc.*, **43**.
Henden, A. A., Terrell, D., Welch, D. and Smith, T. C. 2010, *Bull. Amer. Astron. Soc.*, **42**, 515.
Henden, A. A., Welch, D. L., Terrell, D., and Levine, S. E. 2009, *Bull. Amer. Astron. Soc.*, **41**, 669.
Hoffman, D. I., Harrison, T. E., Coughlin, J. L., McNamara, B. J., Holtzman, J. A., Taylor, G. E., and Vestrand, W. T. 2008, *Astron. J.*, **136**, 1067.
Hoffman, D. I., Harrison, T. E., and McNamara, B. J. 2009, *Astron. J.*, **138**, 466.

Houdashelt, M. L., Bell, R. A., and Sweigart, A. V. 2000, *Astron. J.*, **119**, 1448.
Howell, S. B. 2006, *Handbook of CCD Astronomy*, 2nd ed., Cambridge Univ. Press, Cambridge.
IONDEV SRL. 2021, QtiPlot—Data Analysis and Scientific Visualisation (https://www.qtiplot.com/).
Jayasinghe, T., *et al.* 2018, *Mon. Not. Roy. Astron. Soc.*, **477**, 3145.
Kafka, S. 2021, Observations from the AAVSO International Database (https://www.aavso.org/data-download).
Kallrath, J., and Milone, E. F. 2009, *Eclipsing Binary Stars: Modeling and Analysis*, Springer-Verlag, New York.
Korda, D., Zasche, P., Wolf, M., Kučáková, H., Hoňková, K., and Vraštil, J. 2017, *Astron. J.*, **154**, 30.
Kurucz, R. L. 2002, *Baltic Astron.*, **11**, 101.
Latković, O., Čeki, A., and Lazarević, S. 2021, *Astrophys. J., Suppl. Ser.*, **254**, 10.
Lewandowski, M., Gorecka, M., Maciejewski, G., and Niedzielski, A. 2009, *Open Eur. J. Var. Stars*, **104**, 1.
Li, K., *et al.* 2019, *Res. Astron. Astrophys.*, **19**, 147.
Liu, L. 2021, *Publ. Astron. Soc. Pacific*, **133**, 084202.
Lucy, L. B. 1967, *Z. Astrophys.*, **65**, 89.
Mortara, L., and Fowler, A. 1981, in *Solid State Imagers for Astronomy*, eds. J. C. Geary, D. W. Latham, SPIE, Bellingham, WA, 28.
Minor Planet Observer. 2010, MPO Software Suite (https://minplanobs.org/BdwPub/php/displayhome.php), BDW Publishing, Colorado Springs.
Nelson, R. H. 2009, WDwint56a: Astronomy Software by Bob Nelson[3]
Niedzielski, A., Maciejewski, G., and Czart, K. 2003, *Acta Astron.*, **53**, 281.
O'Connell, D. J. K. 1951, *Publ. Riverview Coll. Obs.*, **2**, 85.
Pecaut, M. J., and Mamajek, E. E. 2013, *Astrophys. J., Suppl. Ser.*, **208**, 9.
Prša, A., and Zwitter, T. 2005, *Astrophys. J.*, **628**, 426.
Qian, S. 2001, *Mon. Not. Roy. Astron. Soc.*, **328**, 635.
Qian, S. 2003, *Mon. Not. Roy. Astron. Soc.*, **342**, 1260.
Ruciński, S. M. 1969, *Acta Astron.*, **19**, 245.
Schlafly, E. F., and Finkbeiner, D. P. 2011, *Astrophys. J.*, **737**, 103.
Shappee, B. J., *et al.* 2014, *Astrophys. J.*, **788**, 48.
Smith, T. C., Henden, A. A., and Starkey, D. R. 2011, in *The Society for Astronomical Sciences 30th Annual Symposium on Telescope Science*, Society for Astronomical Sciences, Rancho Cucamonga, CA, 121.
Software Bisque. 2019, TheSkyX professional edition 10.5.0 (https://www.bisque.com/product/theskyx-pro/).
Terrell, D. 2022, *Galaxies*, **10**, 8.
Terrell, D., and Wilson, R. E. 2005, *Astrophys. Space Sci.*, **296**, 221.
van Hamme, W. 1993, *Astron. J.*, **106**, 2096.
Watson, C., Henden, A. A., and Price, C. A. 2014, AAVSO International Variable Star Index VSX (Watson+, 2006–2014; https://www.aavso.org/vsx).
Wilson, R. E. 1979, *Astrophys. J.*, **234**, 1054.
Wilson, R. E. 1990, *Astrophys. J.*, **356**, 613.
Wilson, R. E., and Devinney, E. J. 1971, *Astrophys. J.*, **166**, 605.
Woźniak, P. R., *et al.* 2004, *Astrophys. J.*, **127**, 2436.

[3] Nelson (2009); https://www.variablestarssouth.org/resources/bob-nelsons-software-tools/software-by-bob-nelson